

# Combined Molecular Dynamics Simulation and Rouse Model Analysis of Static and Dynamic Properties of Unentangled Polymer Melts with Different Chain Architectures

Pu Yao<sup>a,b</sup>, Lu-Kun Feng<sup>a,b</sup>, and Hong-Xia Guo<sup>a,b\*</sup>

<sup>a</sup> Beijing National Laboratory for Molecular Sciences, Joint Laboratory of Polymer Sciences and Materials, State Key Laboratory of Polymer Physics and Chemistry, Institute of Chemistry, Chinese Academy of Sciences, Beijing 100190, China

<sup>b</sup> University of Chinese Academy of Sciences, Beijing 100049, China

 Electronic Supplementary Information

**Abstract** Chain architecture effect on static and dynamic properties of unentangled polymers is explored by molecular dynamics simulation and Rouse mode analysis based on graph theory. For open chains, although they generally obey ideal scaling in chain dimensions, local structure exhibits nonideal behavior due to the incomplete excluded volume (EV) screening, the reduced mean square internal distance (MSID) can be well described by Wittmer's theory for linear chains and the resulting chain swelling is architecture dependent, *i.e.*, the more branches a bit stronger swelling. For rings, unlike open chains they are compact in term of global sizes. Due to EV effect and nonconcatenated constraints their local structure exhibits a quite different non-Gaussian behavior from open chains, *i.e.*, reduced MSID curves do not collapse to a single master curve and fail to converge to a chain-length-independent constant, which makes the direct application of Wittmer's theory to rings quite questionable. Deviation from ideality is further evidenced by limited applicability of Rouse prediction to mode amplitude and relaxation time at high modes as well as the non-constant and mode-dependent scaled Rouse mode amplitudes, while the latter is architecture-dependent and even molecular weight dependent for rings. The chain relaxation time is architecture-dependent, but the same scaling dependence on chain dimensions does hold for all studied architectures. Despite mode orthogonality at static state, the role of cross-correlation in orientation relaxation increases with time and the time-dependent coupling parameter rises faster for rings than open chains even at short time scales it is lower for rings.

**Keywords** Rouse model; Unentangled chains; Architecture; Excluded volume effects

**Citation:** Yao, P.; Feng, L. K.; Guo, H. X. Combined molecular dynamics simulation and rouse model analysis of static and dynamic properties of unentangled polymer melts with different chain architectures. *Chinese J. Polym. Sci.* 2021, 39, 512–524.

## INTRODUCTION

Modern synthesis techniques<sup>[1–3]</sup> have opened many new opportunities to synthesize polymers with complex chain architectures such as ring, star, comb, and so on. Considering that the macroscopic characteristics of polymers are a result of different structural and dynamic behavior occurring over a large range of length and time scales, a deep investigation of the static and dynamic properties of polymer melting with complex internal topologies in terms of local and global scales as well as auto- and cross-correlations would be of critical importance to understanding the polymer architecture effect<sup>[4–6]</sup> and of great practical interest in technical applications,<sup>[7]</sup> but it remains as one of the main challenges in polymer science. Under such circumstances, molecular dynamics (MD) simulation is an invaluable tool to access these desired quantities since every

individual chain can be directly monitored. As such, a MD simulation study of structural and dynamical properties of unentangled polymer chains with different molecular architectures and a quantitative comparison of the observed behavior with the mechanisms already proposed in simplified theories will not just provide important insights into the relationship between the topology of a polymer and its distinctive structural and dynamical behaviors but also clear up some of the confusions. These can be considered as a useful starting point for a systematic study of polymer architecture and further studies would be very beneficial to development of more realistic models for (un)entangled polymers.

According to "Flory ideality hypothesis", in the unentangled polymer melts the excluded volume (EV) interactions are screened on the length scale beyond the diameter of monomers,<sup>[8]</sup> and thus polymer chains behave statistically as ideal chains with Rouse-like chain dynamics. Among various static properties, the mean square internal distance (MSID) is often used to analyze internal structure or conformation of chains, *i.e.*, for the linear polymers in melts it can rep-

\* Corresponding author, E-mail: hxguo@iccas.ac.cn

Received July 18, 2020; Accepted July 31, 2020; Published online September 29, 2020

resent the information of a single chain on all scales independent of the molecular weight.<sup>[9–13]</sup> Recent theoretical calculations and simulation studies on the linear chains have revealed some deviations from the ideal chain behavior due to an incomplete EV screening like the increasing of the scaled MSID to an asymptotic plateau.<sup>[6,14,15]</sup> Moreover, Wittmer *et al.*<sup>[16–18]</sup> proposed an improved theory for linear chains, which considers the above “swelling effect” as a result of the long-range intrachain correlation, a phenomenon manifested as the bond-bond decorrelation behavior unable to be simply described as an exponential decay but rather a power law decay for a larger chemical distance, or more precisely, as a result of the repulsive interactions between segments due to the chain connectivity and the incompressibility. Thus, by analyzing MSID they derive two parameters of effective bond length  $b_e$  and swelling coefficient  $c_s$  for systematic evaluations of the relative deviation from the ideal chain behavior. Unfortunately, to our knowledge, relatively little is known for whether or how the chain architecture affects such deviation from the ideal chain. It should be noted that polymers with nonlinear architectures, *i.e.*, star and comb, can experience some volume exclusions for chain architecture reasons when compared to linear polymers. And the correlation hole in the melt of ring chains is found to be deeper and wider than that of linear chains.<sup>[19]</sup> Therefore, it is of great interest to study the internal structure of polymer chains with nonlinear architectures, in order to gain more insights on the relationship between architecture and conformation properties.

As for polymer dynamics, the well-known Rouse model is commonly employed to describe dynamics of unentangled polymer melts.<sup>[20]</sup> When directly solving the Rouse equations at continuum level, unlike the linear and ring polymers<sup>[19]</sup> the boundary condition relating to the chain topology becomes hard to handle for more complex architectures such as asymmetrical star and comb. On the other hand, with the help of the graph theory, the quantitative descriptions for the chain architecture information are accessible by a Laplacian matrix, solutions of the Rouse equations can thus be derived in discrete form for various architectures. Along this line, a new approach, generalized Gaussian structures (GGS),<sup>[21]</sup> has recently been proposed based on the original Rouse model, which sets up a unified standard to quantify the architecture effect of chain architecture on dynamics properties. Further extension of the GGS model has been developed by Dolgushev *et al.*<sup>[22–24]</sup> to involve the chain stiffness, which provides valuable analytical insights into single-polymer dynamics of semiflexible polymer systems with complex internal topologies. However, when comparing the resulting analytical data with Monte Carlo simulations some discrepancies are observed by Dolgushev *et al.*,<sup>[24]</sup> since the above GGS approach is a single chain model and within this framework many-chain effects as well as excluded volume interactions in real systems are disregarded. Nevertheless, it has been recognized that quantifying polymer dynamics of more involved models at various length scales using a Rouse mode analysis will also contribute significantly to the full understanding of the dynamic behavior of complex polymer systems, in addition to testing the applicability limit of Rouse model. This approach has been applied widely to the analysis of experimental data and simulation data on linear chains.<sup>[25–27]</sup> Unfor-

tunately, to our best knowledge, relatively few efforts have been devoted toward the Rouse mode analysis of MD simulation data through GGS calculations especially for non-linear polymers. Actually, by means of the above more general Rouse mode analysis on MD data, we can measure the relaxation of internal modes of the chains which is essential for our understanding of a hierarchical relaxation processes occurring in real systems, and also check the internal correlations of the chain which continues to elucidate our understanding of how the underlying topologies of real polymeric materials affect their local static properties. Even more excitingly, researches of this kind will offer a chance to test the validity of current theoretical models and help the development of improved theories for polymer dynamics that take into account the excluded volume interactions as well as interactions with other chains which are encountered in real systems but are disregarded in the GGS.

As addressed above, although the Rouse model has been shown to successfully describe the large time and length scale behavior of short polymers in melts, there are still some contrary phenomena observed from experiments and simulations.<sup>[4,28]</sup> The reason for these discrepancies also lies in the fact that Rouse model relies on “Flory ideality hypothesis”, *i.e.*, the chains are assumed to be Gaussian and excluded volume interactions are screened. Furthermore, Masubuchi *et al.*<sup>[5]</sup> observed that the deviations from Rouse model have close relationship with interaction potentials. Additionally, the cross-correlations vanish in Rouse model, but recent experiments<sup>[29,30]</sup> and simulations<sup>[31–33]</sup> show that orientation cross-correlation makes a significant contribution to mechanical relaxation process. For example, Likhtman *et al.*<sup>[32]</sup> proposed a time-dependent coupling parameter  $\kappa(t)$  to quantify the relative importance of cross-correlations during the orientation relaxation and their MD study on linear polymer melts indicated that  $\kappa(t)$  is independent of molecular weight or blend composition and the cross-correlations constitute a prominent fraction about 50% at long time. Very recently, Masubuchi *et al.*<sup>[33]</sup> performed multi-chain slip-link simulations on entangled branched polymers and found  $\kappa(t)$  is virtually identical to that of linear polymers. However, a full understanding of whether or how the chain topology affects the orientation cross-correlation or the deviation from the Rouse model is yet to be achieved. Also, by means of graph theory, the cross-correlation contributions to dynamics properties of polymer chains with various architectures can be studied by orientation correlation functions *via* integrating the orientation of the segments corresponding to the edges of graph.

In this work, to explore the architecture restriction effects on static and dynamic behaviors of unentangled polymer chains, the linear, symmetric star, asymmetric star, comb, and ring polymer melts are investigated by a MD simulation with generic coarse-grained flexible polymer chain model, namely Kremer–Grest (KG) model and the resulting trajectories are analyzed by Rouse model based on graph theory to evaluate the various correlation functions. As a key challenge in a deeper understanding of chain topology, we pay special attention to the deviations of both static properties and dynamics from Flory’s theorem of equilibrated melts of these chains on different time- and space-scales.

## ROUSE MODE ANALYSIS

We note that by the study of the Rouse modes of the chain or Rouse mode analysis we cannot just check the single chain dynamics but also the structural properties of the polymers. Recently, Rouse model was extended to polymers with various architecture<sup>[21,34]</sup> based on graph theory, wherein the linear, ring, star, A-star and comb polymers are viewed as chain graphs with their edges and vertices corresponding to the harmonic springs and beads of polymers, respectively. A connectivity matrix or a Laplacian matrix  $L_G$  can thus be constructed to describe the bonded interactions between neighboring beads.<sup>[35]</sup> In matrix notation, the linearized Langevin equation of motion in the Rouse model can be rewritten as:<sup>[36,37]</sup>

$$\zeta \frac{d\mathbf{R}}{dt} = -\frac{3k_B T}{2b^2} L_G \mathbf{R} + \mathbf{F} \quad (1)$$

where  $\zeta$  denotes monomeric friction coefficient.  $\mathbf{R}$  is the vector for a polymer chain with  $N$  beads and  $\mathbf{R} = [\mathbf{r}_0, \mathbf{r}_1, \dots, \mathbf{r}_i, \dots, \mathbf{r}_{N-2}, \mathbf{r}_{N-1}]^T$  with  $\mathbf{r}_i$  being the position vector of the bead  $i$ . On the right-hand side of Eq. (1),  $k = \frac{3k_B T}{b^2}$  represents the elastic constant of Gaussian entropic elastic springs and  $b$  denotes the average bond length.  $\mathbf{F}$  is the vector of random forces and  $\mathbf{F} = [\mathbf{f}_0, \mathbf{f}_1, \dots, \mathbf{f}_i, \dots, \mathbf{f}_{N-2}, \mathbf{f}_{N-1}]^T$  with the random forces  $\mathbf{f}_i^R(t)$  interrelated through the fluctuation-dissipation theorem:  $\langle \mathbf{f}_{i\alpha}^R(t) \mathbf{f}_{j\beta}^R(t') \rangle = 2k_B T \zeta \delta_{ij} \delta_{\alpha\beta} \delta(t-t')$ ,  $\alpha, \beta = x, y, z$ . One should note here that Eq. (1) may be solved by decoupling into independent normal mode equations via diagonalization of the Laplacian matrix  $L_G$  and transformation of the Cartesian coordinates  $\mathbf{R}$  to the normal coordinates  $\mathbf{X}$ . The linear transformation matrix to diagonalize  $L_G$  is defined as:

$$\mathbf{P} = [\mathbf{p}_0, \mathbf{p}_1, \dots, \mathbf{p}_i, \dots, \mathbf{p}_{N-2}, \mathbf{p}_{N-1}]^T \quad (2)$$

where  $\mathbf{p}_i$  is the  $i^{\text{th}}$  normalized eigenvector and its corresponding eigenvalue is  $\lambda_i$ . The details of derivation of  $\lambda_i$  and  $\mathbf{p}_i$  for our studied chain architectures are provided in the electronic supplementary information (ESI). The normal coordinates are given by a linear transformation  $\mathbf{X} = \mathbf{P}^{-1} \mathbf{R}$  with the Rouse modes  $i = 0, 1, 2, \dots, N-1$ . For the mode  $i=0$ ,  $X_0$  represents the motion of the center of mass of chain and the corresponding eigenvalue is  $\lambda_0=0$ . In this way, the Rouse correlators for all polymers with different architectures evaluate the single chain dynamics and the structural properties of the polymers can be deduced.

For the ideal chain, Rouse modes are independent of each other, the cross-correlations should vanish while the autocorrelation function is expected to decay exponentially with time, so the correlation function is given by

$$\langle X_p(t) X_q(0) \rangle = \delta_{pq} \frac{b^2}{\lambda_p} \exp\left(-\frac{t}{\tau_p}\right) \quad (3)$$

where  $\tau_p$  denotes the characteristic relaxation time of the  $p^{\text{th}}$  mode,

$$\tau_p = \frac{b^2 \zeta}{3\lambda_p k_B T} \quad (4)$$

At  $t=0$  the static correlation of the modes or the Rouse mode amplitudes, *i.e.*, the amplitude of the autocorrelation function of Rouse mode  $p$ , which reflects local chain structure, is expected to obey a simple power law:

$$\langle X_p^2 \rangle = \frac{b^2}{\lambda_p} \quad (5)$$

Additionally, further multiplying the Rouse mode amplitude by the corresponding eigenvalue, the resulting scaled Rouse mode amplitudes ( $\lambda_p \langle X_p^2 \rangle$ ), which is given by the following formula:

$$\lambda_p \langle X_p^2 \rangle = b^2 \quad (6)$$

would allow for comparisons of segment size.

However, when the excluded volume interaction and topological constraint are considered, the normalized time-dependent autocorrelation function can hardly be described by a simple exponential fashion but always be described by a stretched exponential Kohlrausch-Williams-Watts (KWW) function:

$$\frac{\langle X_p(t) \cdot X_p(0) \rangle}{\langle X_p^2 \rangle} = \exp\left[-\left(\frac{t}{\tau_{\text{KWW}p}}\right)^{\beta_p}\right] \quad (7)$$

where two fitting parameters  $\tau_{\text{KWW}p}$  and  $\beta_p$  are the KWW characteristic relaxation time and the stretching exponent of the mode  $p$ . Thus, the effective relaxation time of mode  $p$  is given by

$$\tau_p^{\text{eff}} = \left(\frac{\tau_{\text{KWW}p}}{\beta_p}\right) \Gamma\left(\frac{1}{\beta_p}\right) \quad (8)$$

where  $\Gamma(x)$  is the gamma function.

In this case, to validate the applicability of the Rouse mode analysis, it is important to assess whether the Rouse modes are indeed orthogonal or not. Following the method described in Refs. [38–40] the orthogonality of Rouse modes is estimated by a normalized static ( $t=0$ ) correlation product:

$$X_{pq} = \frac{|\langle \mathbf{X}_p \cdot \mathbf{X}_q \rangle|}{\sqrt{\langle X_p^2 \rangle \langle X_q^2 \rangle}} \quad (9)$$

Accordingly, for the diagonal elements of the correlation matrix, corresponding to  $p=q$ ,  $X_{pq}$  are unity. For the off-diagonal elements  $p \neq q$ ,  $X_{pq}$  should be zero if the modes are orthogonal. Deviation from Rouse model can be detected from the heatmap of the cross-correlation matrix.

## METHODOLOGY

### Model and Simulation Details

Similar to those used in the literatures,<sup>[9,41–43]</sup> the model of the polymer chains we employed in this work is a generic coarse-grained flexible polymer chain model or the so called Kremer-Grest (KG) model. All beads interact *via* a shifted purely repulsive Lennard-Jones (LJ) potential with a cutoff distance of  $r_c = 2^{1/6} \sigma$ :

$$U_{\text{LJ}}(r_{ij}) = \begin{cases} 4\epsilon \left[ \left(\frac{\sigma}{r_{ij}}\right)^{12} - \left(\frac{\sigma}{r_{ij}}\right)^6 + \frac{1}{4} \right], & r_{ij} < r_c \\ 0, & r_{ij} \geq r_c \end{cases} \quad (10)$$

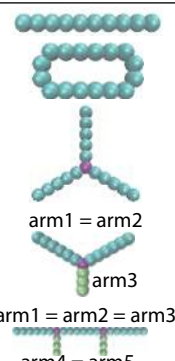
where  $\epsilon$ ,  $\sigma$  and  $r_{ij}$  are the energy scale, the length scale, and the distance between beads, respectively. In addition, the nearest neighbor beads along the chain interact *via* the finitely extensible nonlinear elastic (FENE) potential with the spring constant of  $K = 30\epsilon/\sigma^2$  and the maximal bond length of  $R_0 = 1.5\sigma$ .<sup>[9,41]</sup>

$$U_{\text{Bond}}(r_{ij}) = -\frac{1}{2}KR_0^2 \ln \left[ 1 - \left( \frac{r_{ij}}{R_0} \right)^2 \right], \quad r_{ij} < R_0 \quad (11)$$

In the present study, MD simulations are carried out in a NVT ensemble at the same temperature of  $k_B T/\varepsilon=1.0$  and a constant monomer number density of  $\rho=0.85$ , where  $k_B$  is the Boltzmann constant. We use a Langevin thermostat with a friction constant  $\Gamma = 0.5m/\tau$  to maintain the temperature, wherein  $m$  is the mass of a bead and  $\tau$  is the time scale given by  $\tau = \sigma\sqrt{m/\varepsilon}$ . All simulations are performed using LAMMPS<sup>[44]</sup> with a time step of  $\Delta t=0.01\tau$  and run up to at least  $1 \times 10^8$  MD steps after equilibration. A cubic simulation box with periodic boundary conditions in all dimensions is adopted for each simulation. The studied polymer melts consist of 1000 chains with  $N$  ( $N = 50, 52, 61, 67, 73, 76, 83$ ) beads per chain. Note that the entanglement length ( $N_e$ ) is about 85 for the flexible linear chains<sup>[11,26,45]</sup> verified by stress relaxation data,<sup>[46]</sup> thus the studied chains are unentangled. The architecture and the bead number per chain ( $N$ ) of each system are listed in Table 1. As indicated schematically in this table, for the asymmetric star (A-star) polymers the arm length satisfies  $\text{arm1} = \text{arm2}$ , while for comb polymers the length of each part satisfies  $\text{arm1} = \text{arm2} = \text{arm3}$  and  $\text{arm4} = \text{arm5}$ . To ensure good statistics, each run is repeated at least 8 times and then the results are averaged. Additionally, we should stress that our shortest ring with  $N=50$  is beyond the short limit, below which the single ring will lead to explosion of the system due to strong repulsive forces between intra beads along the chain for Kremer-Grest model.<sup>[47]</sup>

**Table 1** The architecture and the bead number per chain ( $N$ ) of each system.

Architecture	$N$
Linear	50 52 61 67 73 76 83
Ring	50 52 61 67 73 76 83
Star	52 61 67 76 82
A-star	61 67 83
Comb	61 67 73 83



## Observables

To quantify the static and dynamic behaviors of unentangled polymer melts with different chain architectures, besides the chain Rouse modes, we monitor the chain dimensions, positional intrachain correlations, the stress and orientation relaxation functions, and the relevant definitions are given below.

### Intrachain correlations

To learn the intrachain correlations for bead positions along the chain with complex architectures, we can regard the chain architectures as a graph<sup>[21,35]</sup> and calculate the mean square internal distance  $\langle R^2(s, G) \rangle$ , i.e., the average squared distance between two monomers separated by a curvilinear (chemical)

distance  $s$  on the chain graph  $G$ ,

$$\langle R^2(s, G) \rangle = \langle (\mathbf{r}_m - \mathbf{r}_n)^2 \rangle_{\text{Path}(m,n,G)=s} \quad (12)$$

where  $\mathbf{r}_m$  is the position vector of the  $m^{\text{th}}$  monomer.  $\text{Path}(m, n, G)$  is the function to calculate the path length from the  $m^{\text{th}}$  bead to the  $n^{\text{th}}$  bead on the graph  $G$  according to the Floyd-Warshall algorithm<sup>[48]</sup> and all path length equal to  $s$  should be taken into account. The Floyd-Warshall algorithm is given in ESI. Physically,  $\langle R^2(s, G) \rangle$  represents the size of chain segments or sub-chains. For an ideal chain, the probability distribution function of internal distances would follow a Gaussian distribution with  $\langle R^2(s, G) \rangle_{\text{Gauss}} = sb^2$ . One expects that the distribution of internal distances of sufficiently long polymer chains should follow this distribution after the excluded volume becomes vanished. For ring polymers, due to the close-loop geometry the two strands are considered. We suppose that  $S$  denotes the length of shorter strand and the length of the longer strand is  $N - S$ . Thus,  $\langle R^2(s, G) \rangle$  is mostly monitored in terms of the effective length of the strand,  $s$ :<sup>[49]</sup>

$$s = \frac{S(N-S)}{N} \quad \text{with } S \leq \frac{N}{2} \quad \text{and } s \leq \frac{N}{4} \quad (13)$$

By virtue of the concept of effective strand length, one can derive  $\langle R^2(s, G) \rangle_{\text{Gauss}} = sb^2$  for a Gaussian ring.

### Stress and orientation relaxation

The stress-optical law states that the relaxation function of total orientation tensor  $S_{\text{tot}}(t)$  should be proportional to the stress relaxation function  $G(t)$ :

$$G(t) = \frac{1}{\alpha} S_{\text{tot}}(t) \quad (14)$$

where  $\alpha$  is the stress-optical coefficient.  $G(t)$  is calculated at each MD time step according to the Ref. [31]:

$$G(t) = \frac{V}{k_B T} \langle \sigma^{\alpha\beta}(t) \sigma^{\alpha\beta}(0) \rangle \quad (15)$$

where  $\sigma^{\alpha\beta}$  is the stress tensor,  $\alpha, \beta = x, y, z$ ,  $V$  is the volume of simulation box. The orientation tensor of the  $j^{\text{th}}$  molecule is defined as:

$$O_j^{\alpha\beta}(t) = \sum_{i=1}^{N_{\text{bond}}} u_{ij}^{\alpha}(t) u_{ij}^{\beta}(t) \quad (16)$$

where  $N_{\text{bond}}$  is the bond number in chain  $j$ ,  $u_{ij}$  is a bond vector of the  $i^{\text{th}}$  bond in the  $j^{\text{th}}$  chain. The autocorrelation contribution to the total orientation relaxation within the same chain is defined as:

$$A_M(t) = \frac{1}{N_c N_{\text{bond}} k_B T} \sum_i^{N_c} \langle O_i^{\alpha\beta}(t) O_i^{\alpha\beta}(0) \rangle \quad (17)$$

where  $N_c$  is the number of chains in the systems. The total orientation correlation function is given by:

$$S_{\text{tot}}(t) = \frac{1}{N_c N_{\text{bond}} k_B T} \left\langle \sum_{j=1}^{N_c} O_j^{\alpha\beta}(t) \sum_{j=1}^{N_c} O_j^{\alpha\beta}(0) \right\rangle \quad (18)$$

Hence, the cross-correlation function of the orientation can be directly obtained by

$$C_M(t) = S_{\text{tot}}(t) - A_M(t) \quad (19)$$

Finally, the contribution of the cross-correlation effect or coupling effect is described by the time-dependent coupling parameter  $\kappa(t)$ , which is defined as following:

$$\kappa(t) = \frac{C_M(t)}{S_{\text{tot}}(t)} = \frac{S_{\text{tot}}(t) - A_M(t)}{S_{\text{tot}}(t)} \quad (20)$$

Note that all these dynamical correlation functions are calculated by a multiple-tau correlator method<sup>[50]</sup> in order to assure the numerical accuracy and improve the computational efficiency.

## RESULTS AND DISCUSSION

To explore the internal architecture restriction effects on static and dynamic behaviors of unentangled polymer chains, we investigate various structural properties and relaxation characteristics of polymer melts with different architectures by analysing the chain size, positional intrachain correlations, the chain Rouse modes, the stress and orientation relaxation functions.

### Chain Dimensions

The mean square radius of gyration ( $\langle R_g^2 \rangle$ ) values for our studied architectures are presented as a function of molecular weight,  $N$ , in Fig. 1. For a given  $N$ , the chain size of linear polymers is the largest while for rings it is the smallest and the branched ones like (a)symmetrical star and comb polymers lie in-between. Furthermore, as linear polymers can be regarded as asymmetric star (or comb) polymers with the short arm length equal to zero while symmetric star polymers can be regarded as an extension of asymmetric star chains with all arm lengths equal to each other, the overall dimensions of asymmetric star chains are expected to locate between the linear chain and symmetric star chain and display a crossover from linear to symmetric star with the growth of short arm to the long arm length. As illustrated in Fig. 1,  $\langle R_g^2 \rangle$  values of asymmetric star chains are indeed generally in-between linear and symmetric star chains. With the increase of molecular weight  $N$  or corresponding to the increase of the short arm (arm3 shown in Table 1) length, their  $\langle R_g^2 \rangle$  data become closer to the symmetric star chains and the order of  $\langle R_g^2 \rangle$  for a fixed  $N$  is symmetric star  $\leq$  asymmetric star  $<$  linear.

These results are not surprising as the shape of asymmetric

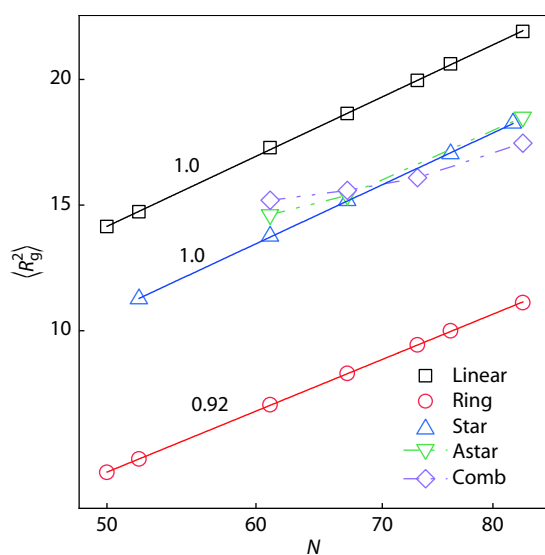


**Fig. 1**  $\langle R_g^2 \rangle$  for all architectures as a function of molecular weight,  $N$ , in logarithmic scale. The solid lines show a fit with  $\langle R_g^2 \rangle \sim N^{2\nu}$  which gives  $\nu=1/2$  for linear and symmetric star polymers and  $\nu=0.46$  for rings.

star chains is not fixed with increasing the length of the short arm towards its long arm counterpart and there exists a shape transition from the linear structure to the symmetric star structure. However, the chain shape of our studied symmetric star or linear polymers is fixed with the increase of molecular weight  $N$  or the simultaneous increase of the three arm lengths. We note that the relative anisotropy  $\kappa^2$  is often employed to characterize the chain shape, which is calculated based on the radius of gyration tensor  $\mathbf{G}$  or its three eigenvalues with  $\lambda_1 > \lambda_2 > \lambda_3$ :<sup>[43,51,52]</sup>

$$\kappa^2 = 1 - 3 \frac{\lambda_1 \lambda_2 + \lambda_2 \lambda_3 + \lambda_3 \lambda_1}{(\lambda_1 + \lambda_2 + \lambda_3)^2} \quad (21)$$

The value of  $\kappa^2$  is normalized and in a range of  $[0, 1]$ , *i.e.*, it takes 1 when all monomers are located on a line while it takes 0 when all monomers are spherically symmetric distributed. As presented in Fig. S2 (in ESI),  $\kappa^2$  is sensitive to the chain architectures. For a given  $N$ ,  $\kappa_{\text{linear}}^2$ ,  $\kappa_{\text{comb}}^2$ ,  $\kappa_{\text{Astar}}^2$ ,  $\kappa_{\text{star}}^2$  and  $\kappa_{\text{ring}}^2$  are in descending order, almost in the same order as the corresponding global chain size  $\langle R_g^2 \rangle$ , indicating the more anisotropy in shape the more extension in size. As expected, our studied linear, ring and symmetric star polymers have a stable value of  $\kappa^2$  with  $\kappa^2 = 0.43$ , 0.24 and 0.29, independent of their molecular weight. However, the relative anisotropy of our studied asymmetric star chains is in-between the linear and symmetric star polymers and follows the order of symmetric star  $\leq$  asymmetric star  $<$  linear, and with the increase of molecular weight  $N$  or corresponding to the increase of the short arm  $\kappa^2$  value is reduced to their symmetric counterpart, in consistency with the above  $\langle R_g^2 \rangle$  results. Despite the shortness of our chains, the open chains with free ends like the linear and symmetric star architectures in the melt they are Gaussian in the sense of a linear scaling (*i.e.*, Flory exponent  $\nu=1/2$ ) of  $R_g$  with  $N$ . Additionally, unlike the symmetric star chains, asymmetric star chains do not show the ideal scaling of  $\langle R_g^2 \rangle \sim N$  within our studied  $N$  range. As for the scaling behavior of our unentangled rings, the derived  $\nu$  approaches to 0.46, indicative of a somewhat compact structure. We note a theoretical value of  $\nu = (1 - \frac{\pi}{3})/2 \approx 0.45$  has been predicted based on the perturbation calculation for unlinked rings.<sup>[53]</sup> However, to reach the asymptotic scaling regime with  $\nu = 1/3$ , characteristic of a compact object, very long ring polymers with  $N$  exceeding a critical ring length of  $N_c$  (see Eq. (6) in Ref. [54]) are required, wherein  $N_c$  for our employed KG model is 6500.

### Internal Structure of the Chains

To obtain the information about the chain conformation for all these chain architectures on all scales in real space, the mean square internal distance  $\langle R^2(s, G) \rangle$  is calculated and the typical results of reduced MSID  $\langle R^2(s, G) \rangle / s$  for polymer melts with  $N=61$  are shown in Fig. 2(a). Additionally, to have a knowledge of molecular weight effect,  $\langle R^2(s, G) \rangle$  data of our studied unentangled linear and ring chains with  $N=61$  and 83 as well as of the entangled linear and ring polymer melts with  $N=151$  ( $N \approx 2N_e$ ) are presented in Fig. S1 (in ESI).

For the open chains, we see  $\langle R^2(s, G) \rangle / s$  increases with  $s$ , indicating that there does exist the correlation between the

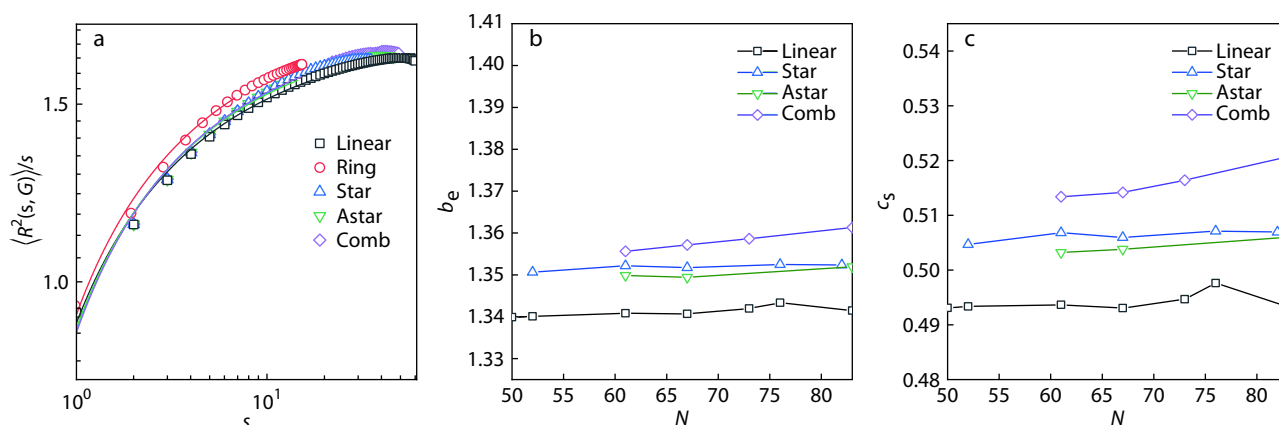


**Fig. 2** (a) The reduced mean square internal distance  $\langle R^2(s, G) \rangle / s$  as a function of  $s$  for chains with  $N=61$  and the fitting curves of Eq. (22), which are represented by open symbols and lines, respectively. (b, c) The derived effective bond length  $b_e$  and swelling coefficient  $c_s$  as a function  $N$  for chains with different architectures.

bond vectors. However, for larger  $s$ ,  $\langle R^2(s, G) \rangle / s$  gradually converges to a constant value, corresponding to the decay of bond vector correlation function. These findings confirm the existence of long-range intrachain correlations or “swelling effect”,<sup>[17]</sup> which is caused by incomplete EV screening but ignored in Gaussian chain model. Moreover, as shown in Fig. 2(a),  $\langle R^2(s, G) \rangle / s$  curves of these open chains display a good collapse within  $s \approx 10$ . However, for larger  $s$ , the reduced MSID curves exhibit a small but still clearly visible architecture dependence: the order of  $\langle R^2(s, G) \rangle / s$  for a fixed  $s$  is comb > symmetric star  $\geq$  asymmetric star > linear. This slight increase behavior is indicative of the fact that open chains with more branches or more free ends are a bit more swollen. Although such phenomena have not been reported so far, it is not unreasonable since the existence of additional topological constraints would lead to a further increase in excluded volume interactions. Moreover, as typically illustrated in Fig. S1(a) (in ESI),  $\langle R^2(s, G) \rangle / s$  curves of the open chains with different chain lengths are almost superimpose, implying that the non-ideal behavior from the EV effect is chain-length independent. We note again that such nonideal behavior was investigated by Wittmer *et al.*,<sup>[17]</sup> who considered the chain swelling effect and proposed corrections for Gaussian chain model and predicted the reduced MSID for linear polymers as

$$\frac{\langle R^2(s, G) \rangle}{s} = b_e^2 \left( 1 - \frac{c_s}{\sqrt{s}} \right) \quad (22)$$

with the effective bond length  $b_e = \lim_{s \rightarrow \infty} \left( \frac{\langle R^2(s, G) \rangle}{s} \right)^{1/2}$ . The idea behind this prediction is that for linear chains due to the incomplete EV screening at short length scales, they are swollen compared to a Gaussian chain of non-interacting subchains. However, for sufficiently long subchains or curvilinear length  $s$ , the distribution function of internal distances approaches to a Gaussian distribution for ideal chains, a linear scaling of  $R^2(s, G)$  in  $s$  or an asymptotic plateau of  $\langle R^2(s, G) \rangle / s$  are expected to reach, as the excluded volume interactions become screened.

Interestingly, the MSID of our studied linear and non-linear open chains can be well described by Eq. (22), as typically in-

dicated by lines in Fig. 2(a) and the resulting fit parameters including effective bond length  $b_e$  and swelling coefficient  $c_s$  for all systems are shown in Figs. 2(b) and 2(c). To minimize the chain-end effects or the reduced self-interactions at chain ends, the fitting is done after eliminating the data around  $s \approx N$ . Herein, we notice several important features. First, for the open chains  $b_e$  and  $c_s$  are almost independent of the molecular weight  $N$ . Particularly, the derived two values for our linear chains are nearly the same as ones reported by Wittmer,<sup>[17]</sup> wherein the flexible bead-spring model with the LJ 9-6 potential is constructed in such a way that the mean bond length is fixed at 0.97 as in our KG model. Another striking observation for these open architectures is that similar to MSID, both  $b_e$  and  $c_s$  display a small but still clearly visible architecture dependence: the more branches the somewhat larger  $b_e$  and  $c_s$ , indicating again a bit stronger swelling effect. For example, the linear molecules have the smallest  $b_e$  and  $c_s$ , the comb ones have the largest  $b_e$  and  $c_s$ , while the (a)symmetric stars are in-between with all data for asymmetric star chains slightly falling below those of symmetric star chains. To our knowledge, such weak architecture-dependent deviation from an ideal chain behavior has not previously been observed.

For the rings, as illustrated in both Fig. 2(a) and Fig. S1(a) (in ESI), although the overall shape of  $\langle R^2(s, G) \rangle / s$  for our studied unentangled ones, *i.e.*,  $N=61$  and 83, is identical to those seen in the open chains; unlike the open chains they do not collapse to a single master curve and fail to converge to a chain-length-independent constant. This is not surprising because in addition to the “swelling effect”<sup>[17]</sup> or the excluded volume effect, the topological constraint like nonconcatenation (uncrossability) constraints between ring chains affects the deviations from an ideal chain behavior. Also, Brown *et al.*<sup>[55]</sup> pointed out that the condition of nonconcatenation is another constraint which leads to the non-Gaussian behavior so that the Gaussian distributions of chain segment size cannot be recovered even at large  $s$  regime after the excluded volume effects gradually vanish. Moreover, if the ring is long enough, the constraints of entanglements will set up. Actually, our results verify the non-Gaussian behavior of rings very different

from that of linear counterparts with respect to local chain structure. Recent simulation results of Lang<sup>[49]</sup> do show that the interpenetrating rings lead to similar non-Gaussian behavior to the linear melts, which is quite different from the non-Gaussian behavior of nonconcatenated ring polymers. For our nonconcatenated rings, such chain-length-dependent non-Gaussian behavior is further evidenced by appearance of a horizontal tangent in  $\langle R^2(s, G) \rangle / s$  curve for the entangled ring ( $N = 151 \approx 2N_e$ ) at  $s \approx 20$ , as shown in Fig. S1(a) (in ESI). Similar behavior has been found in Ref. [49] for the fully entangled rings ( $N > 10N_e$ ) and attributed to the compensation of the remaining effect of excluded volume by topological interactions. Moreover, differences in  $\langle R^2(s, G) \rangle / s$  curve shape between the entangled ring and unentangled rings validate that the static or equilibrium structural properties of our studied unentangled rings are not susceptible to some precursor (crossover) effects of the ultimate reptational dynamics.

Due to the more factors responsible for the non-Gaussian behavior of rings and the resulting different MSD characteristics from open chains, the direct application of Eq. (22) to our rings is questionable. Unfortunately, since there is no way to calculate topological constraints within a Hamiltonian representation,<sup>[56]</sup> it is currently not possible to implement standard analytical results of  $R^2(s)$  for rings. Therefore, we cannot quantify the swelling effect for rings as what has been done for open chains. We may obtain a qualitative conclusion by comparing the reduced MSD at the same curvilinear (chemical) distance, which is denoted as  $S$  thereafter and  $S = s$  for the linear chains and for rings  $S$  is the length of shorter strand. As shown in Fig. S1(b) (in ESI), the subchain size with  $S$  segments of rings is smaller than that of linear polymers, indicating that ring polymers are relatively compact compared with linear counterparts, in consistence with the results from  $R_g$  versus  $N$ . Of course, this is not surprising because there is no free end

but a rather deeper correlation hole in the ring chains.

### Rouse Mode Analysis

We performed the detailed Rouse mode analysis of our MD trajectories to evaluate both static and time-dependent (auto) cross-correlation functions. As another check of the internal structure of chain, we firstly investigate the relationship of the Rouse mode amplitude  $\langle \mathbf{x}_p^2 \rangle$  with its eigenvalue  $\lambda_p$  and the typical results for  $N=61$  are shown in Fig. 3(a). We note that the amplitude of Rouse mode  $p$  is expected to obey a simple power law of Eq. (5) in Rouse model theorem. We see that all the curves nearly collapse to a single master curve. For the lower modes (i.e.,  $\lambda_p < 0.1$ ), the resulting scaling exponent between  $\langle \mathbf{x}_p^2 \rangle$  and  $\lambda_p$  is approximately equal to  $1.041 \pm 0.002$ , quite compatible with the prediction of Rouse model in Eq. (5). For the higher modes (i.e.,  $\lambda_p > 0.1$ ), the Rouse model overestimates  $\langle \mathbf{x}_p^2 \rangle$  for all the architectures. Such deviations in higher mode regime were observed in PE melts<sup>[19]</sup> and entangled linear melts.<sup>[26,57]</sup> Evidently the physical origin is that the original Rouse model ignores the excluded volume interaction, topological constraint, intramolecular correlation, and chain stiffness. For example, to consider the local chain stiffness Binder *et al.*<sup>[14]</sup> proposed a modified Rouse model by replacing the random walk with a free rotation chain model, which can to some extent account for the suppression of correlations below the Rouse prediction.

Nonideal behavior is also evidenced by the non-constant and mode-dependent scaled Rouse mode amplitudes  $\lambda_p \langle \mathbf{x}_p^2 \rangle$ , as typically presented in Fig. 3(b). Note that to study the molecular weight effects, we have performed additional Rouse mode analysis for the ring and linear polymers with  $N=83$  ( $N < N_e$ ) and  $N=151$  ( $N \approx 2N_e$ ) and the corresponding results are included in Fig. 3(b). We stress again that for ideal chains  $\lambda_p \langle \mathbf{x}_p^2 \rangle = b^2$ , which is constantly independent of mode num-

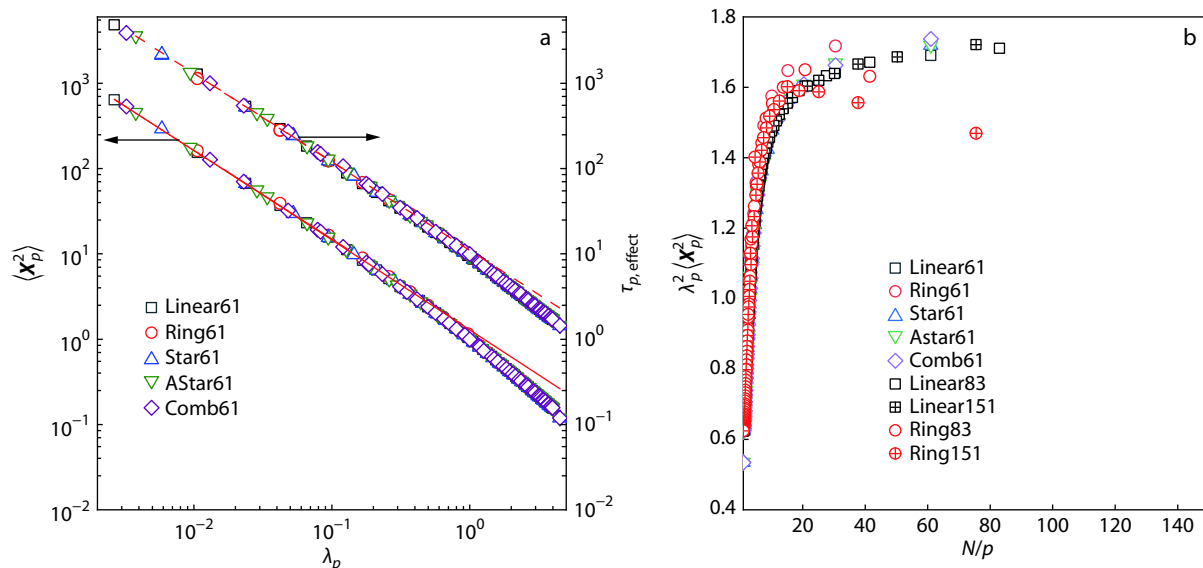


**Fig. 3** (a) Log-log plot of the amplitude of the  $p^{\text{th}}$  mode ( $\langle \mathbf{x}_p^2 \rangle$ ) and its effective relaxation time ( $\tau_{p, \text{effect}}$ ) as a function of eigenvalue  $\lambda_p$  for the systems with  $N=61$ . In addition, the theoretical predictions of Eqs. (4) and (5) are shown as the red dash and solid lines for comparison. (b) Log-log plot of  $\lambda_p \langle \mathbf{x}_p^2 \rangle$  as a function of  $N/p$  for the same samples with  $N=61$  as well as for the linear and ring polymers with  $N=83$  ( $N < N_e$ ) and  $N=151$  ( $N \approx 2N_e$ ).

ber. Although the above scaling relationship between the Rouse mode amplitude and its eigenvalue derived from our MD simulations in Fig. 3(a) seems independent of architectures, the scaled Rouse mode amplitudes  $\lambda_p \langle \chi_p^2 \rangle$ , which allows for comparison of segment length across different architectures, is architecture-dependent. We see that like the reduced mean square internal distance  $\langle R^2(s, G) \rangle / s$  in Fig. 2(a) all open chains of  $N = 61$  exhibit the tendency to level off and roughly fall onto a single curve. Particularly, for linear chains, the data points of different chain lengths almost collapse together and asymptotically approach the effect bond length  $b_e^2$ , very similar to  $\langle R^2(s, G) \rangle / s$  in Fig. S1 (in ESI). As for the ring polymers, we do find that unlike the above linear counterparts, the curves of  $\lambda_p \langle \chi^2(p) \rangle$  versus  $N/p$  depend on the molecular weight  $N$ , also in agreement with the result of  $\langle R^2(s, G) \rangle / s$  in Fig. S1 (in ESI). As addressed above, there are two effects driving the ring polymers to deviate from the Gaussian chains, *i.e.*, the excluded volume effects and the topological constraints. Due to the interplay of the two effects, not only the expected plateau for Gaussian model is not observed but also this non-Gaussian behavior is chain-length-dependent. Moreover, with the increase of molecular weight, the deviation caused by topological constraints becomes more prominent. For example, for the entangled ring of  $N = 151 \approx 2N_e$ , a pronounced peak is found at  $N/p \approx 20$ , similar to the horizontal tangent at  $s \approx 20$  in  $\langle R^2(s, G) \rangle / s$  curve Fig. S1 (in ESI).

Along the line discussed above, it is important to check the normalized static correlation matrixes  $\chi_{pq}$  to further inspect the applicability of the Rouse model. We note again that for the ideal chain Rouse modes are independent of each other and the cross-correlations should vanish. The typical heatmaps of  $\chi_{pq}$  for all architectures with  $N=61$  are presented in Fig. S3 (in ESI). Compared with the diagonal elements, the off-diagonal ones are observed at least 1–2 orders of magnitude smaller than unity, suggesting that the cross-correlation of Rouse modes should have an extremely small effect on static properties and the Rouse modes are approximately orthogonal. Nevertheless, the weak off-diagonal elements exhibit some architecture-dependent, *i.e.*,  $\chi_{pq}$  ( $p \neq q$ ) values for the open chains are generally a bit larger than the rings, wherein the resulting correlation heat map in open architectures shows more pale blue coloring.

Note that for the ideal chain the autocorrelation function of Rouse modes is expected to follow an exponential decay. As typically illustrated in Fig. S4 (in ESI) for our simulated samples of  $N=61$  with different architectures, the normalized autocorrelation functions for all architectures in our simulations are obviously not in a simple exponential decay but can be rather well described by a stretched exponential Kohlrausch-Williams-Watts (KWW) fashion with the stretching exponent  $0 < \beta < 1$  and decreasing with increasing  $p$  as listed in Table S1 (in ESI). Similar behavior has also been found in entangled linear melts.<sup>[26]</sup> The resulting KWW characteristic relaxation time for mode  $p$ ,  $\tau_{KWWp}$ , is listed in Table S2 (in ESI). Since the autocorrelation function of Rouse modes is physically corresponding to the relaxation of  $N/p$  segments, we find the  $\tau_{KWWp}$  values for different architectures at the same  $p$  are

close to each other except at  $p=2$  for the symmetric star polymers. The mode  $p=2$  for star polymers represents the largest relaxation time of star polymers and hence the derived KWW characteristic relaxation time of symmetric star polymers is quite larger than the other ones.

The resulting effective relaxation time of mode  $p$ ,  $\tau_{p, \text{effect}}$  as a function of eigenvalue  $\lambda_p$  is shown in Fig. 3(a). Interestingly, like the static autocorrelation functions (*i.e.*,  $\langle \chi_p^2 \rangle$ ) all curves nearly collapse to a single master curve. For the lower modes, the scaling exponent between  $\tau_{p, \text{effect}}$  and  $\lambda_p$  is  $-1.029 \pm 0.003$ , which is consistent with the Rouse prediction of Eq. (4) as indicated by the red dash line. However, the Rouse model overestimates the relaxation time in higher mode regime. The neutron scattering experiments and atomistic molecular dynamics simulations on PEO melts give the similar results.<sup>[58]</sup> Note that reasons for the deviation of Rouse mode amplitude from the Rouse model also hold for  $\tau_{p, \text{effect}}$ .

To understand the relation between chain size and relaxation time for different chains, we calculate the relaxation time  $\tau_{\text{relax}}$  for the different architectures based on the effective time of the auto-correlation function, that is, Eq. (8), for the first mode of each chain (Note that relaxation time can also be derived from the autocorrelation function of the vector with the largest end-to-end distance, a detailed discussion of the different relaxation time can be found in Ref. [59]). The resulting relaxation time is plotted as a function of molecular weight  $N$  in Fig. 4(a) and mean-square radius of gyration  $\langle R_g^2 \rangle$  in Fig. 4(b).

We can see that with the same molecular weight the relaxation time is architecture dependent.  $\tau_{\text{relax}}$  of linear polymers is the largest while rings take the least time to relax and the branched ones like (a)symmetrical star and comb polymers lie in-between, in the opposite to the order of the chain dimensions  $\langle R_g^2 \rangle$  and the relative anisotropy of chain shape  $\kappa^2$ . For the asymmetrical star and comb polymers, their relaxation time varies between those of linear and (perturbed) symmetric star chains. With the increase of molecular weight  $N$  or corresponding to the increase of the short arm (arm3 for asymmetric star and arm4 or arm5 for comb shown in Table 1) length, their  $\tau_{\text{relax}}$  data become closer to the (perturbed) symmetric star chains and the order of  $\tau_{\text{relax}}$  for a fixed  $N$  is (perturbed)symmetric star  $\leq$  asymmetric star  $<$  comb  $<$  linear, in the almost same tendency as  $\langle R_g^2 \rangle$  and  $\kappa^2$ . As for the scaling behavior of the relaxation time  $\tau_{\text{relax}}$  with molecular weight  $N$ , Rouse theory predicts  $\tau_{\text{relax}} \sim N^{2.0}$  for linear, ring, and symmetric star polymers. However, a little deviation is observed for our studied systems, *i.e.*, the power laws for linear and (perturbed)symmetric star polymers are  $\tau_{\text{relax}} \sim N^{2.36 \pm 0.01}$  and  $\tau_{\text{relax}} \sim N^{2.22 \pm 0.02}$ , respectively. Similar scaling of  $\tau_{\text{relax}} \sim N^{2.26}$  has been reported for linear polymers in Ref. [60], wherein a critical test of the KG model on the scaling laws of the polymer melts was performed.<sup>[60]</sup> Additionally, such small deviation from Rouse theory is found in the united-atom model of polyethylene (PE)<sup>[61]</sup> with  $\tau_{\text{relax}} \sim N^{2.1}$  for  $N < N_e$ . This deviation might come from the strong excluded volume effect, which is provided by the LJ force and leads to the collisions between hard-core particles no longer equal to the Gaussian random force.<sup>[61]</sup> As for the ring polymers, the res-



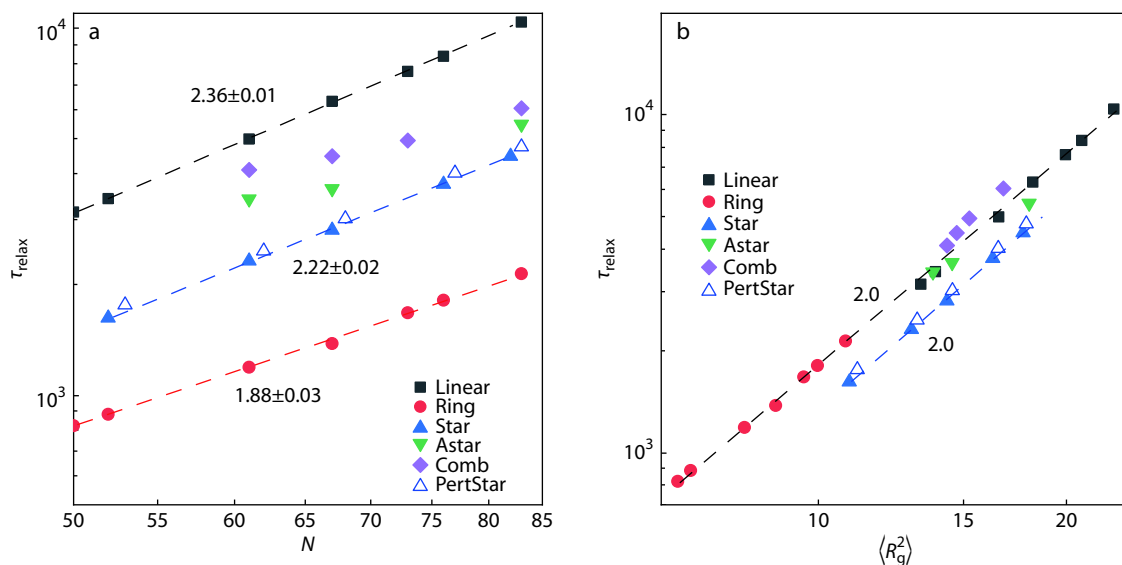


**Fig. 4** The relaxation time  $\tau_{\text{relax}}$  as a function of (a) molecular weight  $N$  and (b) chain dimension  $\langle R_g^2 \rangle$  for our studied unentangled polymers with different architectures. Note that results of the perturbed symmetric star polymers, that is, a kind of weak asymmetric star polymers by inserting an additional bead in one arm of the symmetric star chain to break the chain symmetry, is also shown for comparison.

ulting scaling law is  $\tau_{\text{relax}} \sim N^{1.88 \pm 0.03}$ , quite similar to the scaling of  $\tau_{\text{relax}} \sim N^{1.9}$  found in the unentangled PEO melts,<sup>[62]</sup> and the resulting smaller scaling exponent than the open chains arises from the fast diffusion of ring polymers. Besides, the different power law behaviors could be relevant with the architecture-dependent or the molecular weight dependent effective friction constant. We note that in Rouse theory the friction constant is independent of chain architecture or molecular weight. However, recent experiments and simulations<sup>[41,63–65]</sup> show the correlation-hole interactions<sup>[66]</sup> and the viscoelastic hydrodynamic effects<sup>[67]</sup> result in deviations from Rouse theory like the subdiffusion behavior<sup>[68]</sup> in the mean-square displacement of the center-of-mass of chain. The friction constant of linear polymers is found to increase with molecular weight<sup>[64]</sup> and quite larger than that for ring polymers.<sup>[19]</sup>

When the relaxation time  $\tau_{\text{relax}}$  is plotted as a function of the chain size  $\langle R_g^2 \rangle$  in Fig. 4(b), we find the architecture dependence becomes weaker.<sup>[47,59]</sup> All data points almost lie around the master curve except for the symmetric star and the perturbed symmetric star polymers which fall slightly below, however the same scaling of  $\tau_{\text{relax}}(N) \sim \langle R_g^2(N) \rangle^{2.0}$  holds for all studied systems.

### Orientalional Relaxation Function

Recent simulations on both linear and entangled branched polymers indicated although each individual chain obeys Rouse dynamics, the cross-correlation between the chains is not negligible.<sup>[32,33,69,70]</sup> Orientation correlation function is particularly relevant to the mechanical and dielectric relaxations. To explore the chain architecture effect on orientational relaxation, we firstly check the stress-optical law which tells the relationship between the time-dependent relaxation modulus  $G(t)$  and total orientation correlation function  $S_{\text{tot}}(t)$ . As typically

indicated by Fig. 5, the stress optical law works in our systems, *i.e.*, the two relaxation functions  $G(t)$  and  $S_{\text{tot}}(t)$  become proportional to each other after about  $30\tau$ , which corresponds to the time scale of the bond relaxation and glassy modes.<sup>[31]</sup> The stress-optical coefficient  $\alpha$  derived by Likhtman in Ref. [32] for standard KG model systems of linear chains is 0.0885 and  $\alpha$  is independent of molecular weight and blend composition. Here roughly the same magnitude of  $\alpha$  applies to our systems with different chain architectures. Therefore, the stress-optical coefficient is independent of chain topologies and molecular weight in polymer melts.

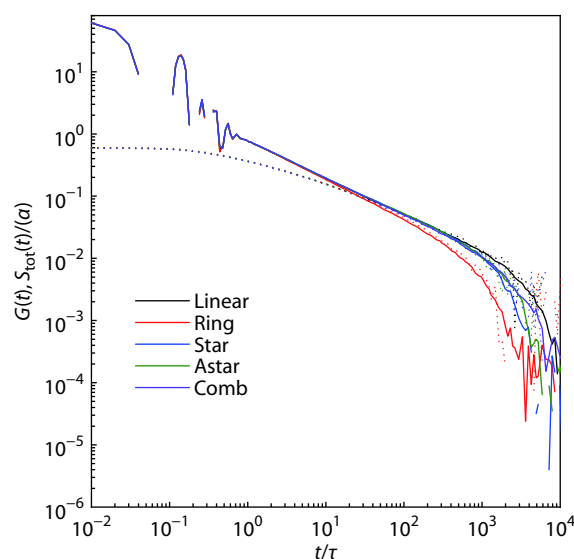


**Fig. 5** Stress (solid lines) and total orientation (dash lines) relaxation functions of  $G(t)$  and  $S_{\text{tot}}(t)$  for all the architectures with a given molecular weight of  $N=61$ .

We note again that the cross-correlation contribution to the orientation correlation is neglected in the Rouse model. To explore the cross-correlation role in the total orientation relaxation in our MD samples, we plot total orientation correlation  $S_{\text{tot}}(t)$  and autocorrelation contribution  $A_M(t)$  in Fig. 6(a) and the corresponding time-dependent coupling parameter  $\kappa(t)$  in Fig. 6(b).

For each studied architecture  $A_M(t)$  nearly overlaps with  $S_{\text{tot}}(t)$  at short time but  $A_M(t)$  turns to relax faster than  $S_{\text{tot}}(t)$  at long time, indicating that the role of cross-correlations increases with time. Additionally, we find that the relaxation of  $A_M(t)$  after about  $10\tau$  is clearly faster for ring-shaped chain than for open chains, which may suggest that the relative importance of cross-correlations in total orientational relaxation function will grow faster with time in rings than in the open-chain counterparts. Indeed, as typically illustrated in Fig. 6(b), the cross-correlation role in the total orientation relaxation seems to grow with time and such growth becomes more pronouncedly for rings after about  $10\tau$ . For example, the time-dependent coupling parameter  $\kappa(t)$  for all the architectures increases from about 12% at  $t=0$  to about 50% at later time. Recent MD simulations on linear polymers<sup>[32]</sup> and multi-chain slip-link simulations<sup>[33,71]</sup> on star-branched and H-branched polymers also give similar results. Meanwhile, we see all the curves of  $\kappa(t)$  are roughly overlapped of each other except for ring polymers, *i.e.*, rings have the lowest  $\kappa(t)$  at short time scales but the situation is reversed after about  $10\tau$ . Additionally, by comparing the  $\kappa(t)$  results of our rings with  $N=61$  and 83 we find that like the open chains such as linear<sup>[32]</sup> and branched ones,<sup>[33,71,72]</sup>  $\kappa(t)$  of ring polymers is independent of the molecular weight.

The origin of orientational cross correlation has been conjectured to be a coupling in the chain dynamics through the excluded volume interactions.<sup>[72]</sup> Masubuchi *et al.*<sup>[33,71,72]</sup> sug-

gested that  $\kappa(t)$  is affected by the density fluctuations due to the incompressibility. Cao *et al.*<sup>[32]</sup> pointed out that any static calculations can just provide the information of  $\kappa(0)$ , whereas the important long-time coupling can be only obtained by dynamics calculations. On the one hand, we note that the coupling at time zero,  $\kappa(0)$ , represents the influence of cross-correlation part on static properties.<sup>[32]</sup> The  $\kappa(0)$  extrapolated from curves in Fig. 6(b) should be very small and lowest for rings, consistent with the result of small but weak architecture-dependent cross-correlation amplitude  $\chi_{ppq}$ . This finding is related to the chain correlation hole, which is deeper for rings and thus may lead to the stronger local intra-ring correlations and enhances the relative role of auto-correlations at short time scales during orientational relaxation of rings. On the other hand, the effective pressure exerted on individual ring chains *via* nonconcatenation constraints between ring chains may slow down the inter-ring or cross-correlation relaxation so that rings can relax their intra-coil much faster than relax their inter-coil correlations (the faster decay of  $A_M(t)$  for rings after about  $10\tau$ ) and their  $\kappa(t)$  tends to rise faster than the open-chains at late time. To test these ideas, we attempt to extract the (dynamic) correlation information of inter-polymers, and more details can be found in ESI. As indicated by Fig. S5 (in ESI), for the rings the mutual (inter-ring) interpenetration is less pronounced but relaxes more slowly, indicative of a deeper correlation hole but a suppressed inter-ring correlation relaxation when compared with the linear-chain counterpart. The correlation hole effect weakens the relative role of cross-correlations at short time scales during orientational relaxation of rings, while an enhanced mutual correlation is responsible for the faster growth of  $\kappa(t)$  with time and even becoming more significant than linear polymers at later time.

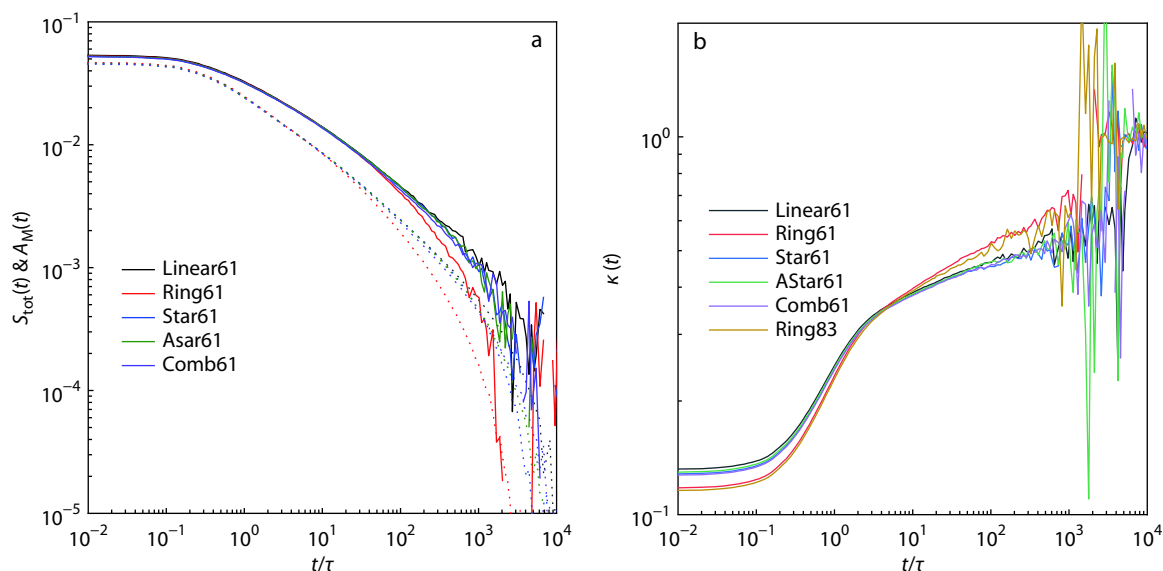


**Fig. 6** (a) The total (solid lines) and the auto-correlations (dash lines) of chain orientation relaxation functions of  $S_{\text{tot}}(t)$  and  $A_M(t)$  for all the architectures with a given molecular weight of  $N=61$ . (b) The time-dependent coupling parameter  $\kappa(t)$  for all the architectures with a given molecular weight of  $N=61$ . Note that in order to have a knowledge of the molecular weight effects on  $\kappa(t)$  for our studied unentangled ring polymers, we include the  $\kappa(t)$  results of our ring polymer melt with molecular weight  $N=83$  in (b).

## CONCLUSIONS

In conclusion, by a combined MD simulation and detailed Rouse analysis based on graph theory, the chain architecture effects on static and dynamic behaviors of unentangled polymers are investigated. For the global sizes of chains, at a given molecular weight  $N$ ,  $\langle R_g^2 \rangle$  is the largest for linear polymers while it is the smallest for rings and the branched ones like (a)symmetrical star and comb polymers lie in-between. Furthermore,  $\langle R_g^2 \rangle$  of asymmetric star chains generally lies in-between linear and symmetric star chains, and the order of  $\langle R_g^2 \rangle$  for a fixed  $N$  is symmetric star  $\leq$  asymmetric star  $<$  linear. The architecture dependent chain dimension is closely relevant to the chain shape. For a given  $N$ , the relative anisotropy  $\kappa^2$  is sensitive to the chain architectures. For example, at a given  $N$ ,  $\kappa_{\text{linear}}^2$ ,  $\kappa_{\text{comb}}^2$ ,  $\kappa_{\text{Astar}}^2$ ,  $\kappa_{\text{star}}^2$  and  $\kappa_{\text{ring}}^2$  are in descending order, almost in the same order as  $\langle R_g^2 \rangle$ , indicating the more anisotropy in shape the more extension in size. Particularly, like above  $\langle R_g^2 \rangle$  result the relative anisotropy of our studied asymmetric star chains is in-between the linear and symmetric star polymers and follows the order of symmetric star  $\leq$  asymmetric star  $<$  linear. Although the open chains like linear and symmetric star architectures obey the ideal scaling, rings are in a somewhat compact non-Gaussian structure with a Flory exponent  $\nu = 0.46 < 1/2$ .

Such architecture dependence is also reflected in the local chain structure, which exhibits some deviations from the ideal chain behavior. For the open chains, reduced MSID curves prove the existence of long-range intrachain correlations or incomplete EV screening and can be well described by Wittmer's theory for linear chains, and the resulting chain swelling is architecture dependent but chain-length independent, *i.e.*, the more branches a bit stronger swelling. As for the rings, due to the EV effect and nonconcatenated constraints, reduced MSID curves exhibit a quite different non-Gaussian behavior from open chains, *i.e.*, unlike the open chains reduced MSID curves do not collapse to a single master curve and fail to converge to a chain-length-independent constant. Hence, more factors (let alone constraints of entanglements which set up if the ring is long enough) responsible for the non-Gaussian behavior of rings and the resulting different MSID characteristics from open chains make the direct application of Wittmer's theory to our rings quite questionable.

Additionally, although the Rouse modes are approximately orthogonal, the weak off-diagonal elements of static correlation product exhibit some architecture-dependence. Also, due to neglect of the excluded volume interaction, topological constraint and intramolecular correlation, the scaling predictions of the Rouse model overestimate mode amplitude and relaxation time at high modes (or local length-scale). Such nonideal behavior is detected again by the non-constant and mode-dependent scaled Rouse mode amplitudes, which is architecture-dependent and even becomes molecular weight dependent for rings. Furthermore, the relaxation time of whole chain is architecture dependent. For example,  $\tau_{\text{relax}}$  of linear polymers is the largest while it is the least for rings and the branched ones like (a)symmetrical star and comb polymers lie in-between, in agreement with the order

of the chain dimensions  $\langle R_g^2 \rangle$  and the relative anisotropy of chain shape  $\kappa^2$ , indicating the more anisotropy in shape the more extension in size and the faster chain relaxation. Particularly,  $\tau_{\text{relax}}$  of asymmetrical star and comb polymers vary between those of linear and (perturbed) symmetric star chains, and the order of  $\tau_{\text{relax}}$  for a fixed  $N$  is (perturbed) symmetric star  $\leq$  asymmetric star  $<$  comb  $<$  linear, in the almost same tendency as  $\langle R_g^2 \rangle$  and  $\kappa^2$ . Although the scaling exponents of  $\tau_{\text{relax}}$  with  $N$  are architecture-dependent, the same scaling of  $\tau_{\text{relax}}(N) \sim \langle R_g^2(N) \rangle^{2.0}$  holds for all studied architectures.

Consistent with the recent work on linear<sup>[32]</sup> and branched polymers,<sup>[33]</sup> the role of cross-correlation in orientational relaxation increases with time and the time-dependent coupling parameter  $\kappa(t)$  is increased from about 12% at  $t = 0$  to about 50% at later time. Interestingly, although  $\kappa(t)$  is architecture-independent for the open chains,  $\kappa(t)$  for rings is lower at short time scales but rises faster at later time than open chains. Furthermore, like the open chains such as linear and branched ones,  $\kappa(t)$  of ring polymers is independent of the molecular weight. The stronger correlation hole effect weakens the relative role of cross-correlations at short time scales during orientational relaxation of rings, while an enhanced mutual correlation is responsible for the faster growth of  $\kappa(t)$  with time. These results demonstrate the architecture dependent nonGaussian behavior, while up to now only the linear chains have revealed such deviation. Researches of this kind will help for the development of modified Rouse model to account for the topological information and the internal architecture restriction effects as well as the excluded volume interaction. It is worthy to note that to our knowledge it is the first time to successfully adopt the combined MD simulation and graph theory to explore chain architecture effects, which provides a route to investigate polymers with any chain-topology.

## Electronic Supplementary Information

Electronic supplementary information (ESI) is available free of charge in the online version of this article at <https://doi.org/10.1007/s10118-020-2489-4>.

## ACKNOWLEDGMENTS

This work was financially supported by the National Natural Science Foundation of China (Nos. 21790343, 21574142, and 21174154) and the National Key Research and Development Program of China (No. 2016YFB1100800).

## REFERENCES

- 1 Hadjichristidis, N.; Pitsikalis, M.; Pispas, S.; Iatrou, H. Polymers with complex architecture by living anionic polymerization. *Chem. Rev.* **2001**, *101*, 3747–92.
- 2 Hadjichristidis, N.; Iatrou, H.; Pitsikalis, M.; Mays, J. Macromolecular architectures by living and controlled/living polymerizations. *Prog. Polym. Sci.* **2006**, *31*, 1068–1132.
- 3 Grubbs, R. B.; Grubbs, R. H. 50<sup>th</sup> Anniversary perspective: living

- polymerization—emphasizing the molecule in macromolecules. *Macromolecules* **2017**, *50*, 6979–6997.
- 4 Paul, W.; Smith, G. D.; Yoon, D. Y. Static and dynamic properties of a  $n\text{-C}_{100}\text{H}_{202}$  melt from molecular dynamics simulations. *Macromolecules* **1997**, *30*, 7772–7780.
  - 5 Masubuchi, Y.; Takata, H.; Amamoto, Y.; Yamamoto, T. Relaxation of rouse modes for unentangled polymers obtained by molecular simulations. *Nihon Reorogi Gakk* **2018**, *46*, 171–178.
  - 6 Fatkullin, N. F.; Shakirov, T. M.; Balakirev, N. A. Why does the rouse model fairly describe the dynamic characteristics of polymer melts at molecular masses below critical mass? *Polym. Sci., Ser. A* **2010**, *52*, 72–81.
  - 7 Vasile, C.; Pascu, M. *Practical guide to polyethylene*. Rapra Technology Limited, **2005**.
  - 8 Flory, P. J. *Statistical mechanics of chain molecules*. Interscience: New York, **1969**.
  - 9 Auhl, R.; Everaers, R.; Grest, G. S.; Kremer, K.; Plimpton, S. J. Equilibration of long chain polymer melts in computer simulations. *J. Chem. Phys.* **2003**, *119*, 12718–12728.
  - 10 Zhang, G. J.; Moreira, L. A.; Stuehn, T.; Daoulas, K. C.; Kremer, K. Equilibration of high molecular weight polymer melts: a hierarchical strategy. *ACS Macro Lett.* **2014**, *3*, 198–203.
  - 11 Moreira, L. A.; Zhang, G. J.; Muller, F.; Stuehn, T.; Kremer, K. Direct equilibration and characterization of polymer melts for computer simulations. *Macromol. Theory Simul.* **2015**, *24*, 419–431.
  - 12 Svaneborg, C.; Karimi-Varzaneh, H. A.; Hojdis, N.; Fleck, F.; Everaers, R. Multiscale approach to equilibrating model polymer melts. *Phys. Rev. E* **2016**, *94*, 032502.
  - 13 Sliozberg, Y. R.; Kroger, M.; Chantawansri, T. L. Fast equilibration protocol for million atom systems of highly entangled linear polyethylene chains. *J. Chem. Phys.* **2016**, *144*, 154901.
  - 14 Kreer, T.; Baschnagel, J.; Müller, M.; Binder, K. Monte Carlo simulation of long chain polymer melts: crossover from Rouse to reptation dynamics. *Macromolecules* **2001**, *34*, 1105–1117.
  - 15 Hsu, H. P. Lattice Monte Carlo simulations of polymer melts. *J. Chem. Phys.* **2014**, *141*, 234901.
  - 16 Wittmer, J. P.; Beckrich, P.; Johner, A.; Semenov, A. N.; Obukhov, S. P.; Meyer, H.; Baschnagel, J. Why polymer chains in a melt are not random walks. *Europhys. Lett.* **2007**, *77*, 56003.
  - 17 Wittmer, J. P.; Beckrich, P.; Meyer, H.; Cavallo, A.; Johner, A.; Baschnagel, J. Intramolecular long-range correlations in polymer melts: the segmental size distribution and its moments. *Phys. Rev. E* **2007**, *76*, 011803.
  - 18 Wittmer, J. P.; Meyer, H.; Baschnagel, J.; Johner, A.; Obukhov, S.; Mattioni, L.; Muller, M.; Semenov, A. N. Long range bond-bond correlations in dense polymer solutions. *Phys. Rev. Lett.* **2004**, *93*, 147801.
  - 19 Tsolou, G.; Stratikis, N.; Baig, C.; Stephanou, P. S.; Mavrantzas, V. G. Melt structure and dynamics of unentangled polyethylene rings rouse theory, atomistic molecular dynamics simulation, and comparison with the linear analogues. *Macromolecules* **2010**, *43*, 0692–10713.
  - 20 Doi, M.; Edwards, S. F. *The theory of polymer dynamics*. Oxford University Press, **1988**.
  - 21 Gurtovenko, A. A.; Blumen, A. Generalized gaussian structures: models for polymer systems with complex topologies. *Adv. Polym. Sci.* **2005**, *182*, 171–282.
  - 22 Dolgushev, M.; Blumen, A. Dynamics of semiflexible treelike polymeric networks. *J. Chem. Phys.* **2009**, *131*, 044905.
  - 23 Dolgushev, M.; Berezovska, G.; Blumen, A. Cospectral polymers: differentiation via semiflexibility. *J. Chem. Phys.* **2010**, *133*, 154905.
  - 24 Dolgushev, M.; Berezovska, G.; Blumen, A. Branched semiflexible polymers: theoretical and simulation aspects. *Macromol. Theory Simul.* **2011**, *20*, 621–644.
  - 25 Paul, W.; Smith, G. D.; Yoon, D. Y.; Farago, B.; Rathgeber, S.; Zirkel, A.; Willner, L.; Richter, D. Chain motion in an unentangled polyethylene melt: a critical test of the rouse model by molecular dynamics simulations and neutron spin echo spectroscopy. *Phys. Rev. Lett.* **1998**, *80*, 2346–2349.
  - 26 Kalathi, J. T.; Kumar, S. K.; Rubinstein, M.; Grest, G. S. Rouse mode analysis of chain relaxation in homopolymer melts. *Macromolecules* **2014**, *47*, 6925–6931.
  - 27 Colmenero, J. A generalized rouse incoherent scattering function for chain dynamics of unentangled polymers in dynamically asymmetric blends. *Macromolecules* **2013**, *46*, 5363–5370.
  - 28 Smith, G. D.; Paul, W.; Monkenbusch, M.; Richter, D. On the non-gaussianity of chain motion in unentangled polymer melts. *J. Chem. Phys.* **2001**, *114*, 4285–4288.
  - 29 Graf, R.; Heuer, A.; Spiess, H. W. Chain-order effects in polymer melts probed by  $^1\text{H}$  double-quantum NMR spectroscopy. *Phys. Rev. Lett.* **1998**, *80*, 5738–5741.
  - 30 Ylitalo, C. M.; Kornfield, J. A.; Fuller, G. G.; Pearson, D. S. Molecular-weight dependence of component dynamics in bidisperse melt rheology. *Macromolecules* **1991**, *24*, 749–758.
  - 31 Likhtman, A. E.; Sukumaran, S. K.; Ramirez, J. Linear viscoelasticity from molecular dynamics simulation of entangled polymers. *Macromolecules* **2007**, *40*, 6748–6757.
  - 32 Cao, J.; Likhtman, A. E. Time-dependent orientation coupling in equilibrium polymer melts. *Phys. Rev. Lett.* **2010**, *104*, 207801.
  - 33 Masubuchi, Y.; Pandey, A.; Amamoto, Y.; Uneyama, T. Orientational cross correlations between entangled branch polymers in primitive chain network simulations. *J. Chem. Phys.* **2017**, *147*, 184903.
  - 34 Qi, Y.; Dolgushev, M.; Zhang, Z. Dynamics of semiflexible recursive small-world polymer networks. *Sci. Rep.* **2014**, *4*, 7576.
  - 35 Yang, Y. Z.; Qiu, F.; Zhang, H. D.; Yang, Y. L. The rouse dynamic properties of dendritic chains: a graph theoretical method. *Macromolecules* **2017**, *50*, 4008–4022.
  - 36 Hsu, H. P.; Kremer, K. Detailed analysis of rouse mode and dynamic scattering function of highly entangled polymer melts in equilibrium. *Eur. Phys. J. Spec. Top.* **2017**, *226*, 693–703.
  - 37 Likhtman, A. E.; Ponmurugan, M. Microscopic definition of polymer entanglements. *Macromolecules* **2014**, *47*, 1470–1481.
  - 38 Downey, J. P. Static and dynamic scaling properties of single, self-avoiding polymer chains in two dimensions via the bond fluctuation method of Monte Carlo simulation. *Macromolecules* **1994**, *27*, 2929–2932.
  - 39 Panja, D.; Barkema, G. T. Rouse modes of self-avoiding flexible polymers. *J. Chem. Phys.* **2009**, *131*, 154903.
  - 40 Rauscher, P. M.; Rowan, S. J.; de Pablo, J. J. Topological effects in isolated poly[ $n$ ]catenanes: molecular dynamics simulations and rouse mode analysis. *ACS Macro Lett.* **2018**, *7*, 938–943.
  - 41 Kremer, K.; Grest, G. S. Dynamics of entangled linear polymer melts: a molecular-dynamics simulation. *J. Chem. Phys.* **1990**, *92*, 5057–5086.
  - 42 Kopf, A.; Dünweg, B.; Paul, W. Dynamics of polymer “isotope” mixtures: molecular dynamics simulation and rouse model analysis. *J. Chem. Phys.* **1997**, *107*, 6945–6955.
  - 43 Khabaz, F.; Khare, R. Effect of chain architecture on the size, shape, and intrinsic viscosity of chains in polymer solutions: a molecular simulation study. *J. Chem. Phys.* **2014**, *141*, 214904.
  - 44 Plimpton, S. Fast parallel algorithms for short-range molecular dynamics. *J. Comput. Phys.* **1995**, *117*, 1.
  - 45 Everaers, R.; Sukumaran, S. K.; Grest, G. S.; Svaneborg, C.; Sivasubramanian, A.; Kremer, K. Rheology and microscopic topology of entangled polymeric liquids. *Science* **2004**, *303*, 823–826.
  - 46 Hou, J. X.; Svaneborg, C.; Everaers, R.; Grest, G. S. Stress relaxation in entangled polymer melts. *Phys. Rev. Lett.* **2010**, *105*, 068301.

- 47 Xu, X.; Chen, J.; An, L. Simulation studies on architecture dependence of unentangled polymer melts. *J. Chem. Phys.* **2015**, *142*, 074903.
- 48 West, D. B. *Introduction to graph theory*. Prentice hall Upper Saddle River, **2001**.
- 49 Lang, M. Ring conformations in bidisperse blends of ring polymers. *Macromolecules* **2013**, *46*, 1158–1166.
- 50 Ramirez, J.; Sukumaran, S. K.; Vorselaars, B.; Likhtman, A. E. Efficient on the fly calculation of time correlation functions in computer simulations. *J. Chem. Phys.* **2010**, *133*, 154103.
- 51 Arkin, H.; Janke, W. Gyration tensor based analysis of the shapes of polymer chains in an attractive spherical cage. *J. Chem. Phys.* **2013**, *138*, 054904.
- 52 Blavatska, V.; Janke, W. Shape anisotropy of polymers in disordered environment. *J. Chem. Phys.* **2010**, *133*, 184903.
- 53 Brereton, M. G.; Vilgis, T. A. The statistical mechanics of a melt of polymer rings. *J. Phys. A: Math. Gen.* **1995**, *28*, 1149–1167.
- 54 Halverson, J. D.; Lee, W. B.; Grest, G. S.; Grosberg, A. Y.; Kremer, K. Molecular dynamics simulation study of nonconcatenated ring polymers in a melt. I. Statics. *J. Chem. Phys.* **2011**, *134*, 204904.
- 55 Brown, S.; Szamel, G. Computer simulation study of the structure and dynamics of ring polymers. *J. Chem. Phys.* **1998**, *109*, 6184–6192.
- 56 Obukhov, S.; Johner, A.; Baschnagel, J.; Meyer, H.; Wittmer, J. P. Melt of polymer rings: the decorated loop model. *Europhys. Lett.* **2014**, *105*, 48005.
- 57 Hsu, H. P.; Kremer, K. Static and dynamic properties of large polymer melts in equilibrium. *J. Chem. Phys.* **2016**, *144*, 154907.
- 58 Brodeck, M.; Alvarez, F.; Arbe, A.; Juranyi, F.; Unruh, T.; Holderer, O.; Colmenero, J.; Richter, D. Study of the dynamics of poly(ethylene oxide) by combining molecular dynamic simulations and neutron scattering experiments. *J. Chem. Phys.* **2009**, *130*, 094908.
- 59 Hu, Y. F.; Xue, K. L.; Yu, X. C.; Hou, J. X. The relaxation times of unentangled polymer melts with different molecular architectures. *J. Polym. Res.* **2019**, *26*, 192.
- 60 Takahashi, K. Z.; Yamato, N.; Yasuoka, K.; Masubuchi, Y. Critical test of bead-spring model to resolve the scaling laws of polymer melts: a molecular dynamics study. *Mol. Simul.* **2017**, *43*, 1196–1201.
- 61 Takahashi, K. Z.; Nishimura, R.; Yasuoka, K.; Masubuchi, Y. Molecular dynamics simulations for resolving scaling laws of polyethylene melts. *Polymers* **2017**, *9*, 24.
- 62 Tsalikis, D. G.; Alatas, P. V.; Peristeras, L. D.; Mavrantzas, V. G. Scaling laws for the conformation and viscosity of ring polymers in the crossover region around Me from detailed molecular dynamics simulations. *ACS Macro Lett.* **2018**, *7*, 916–920.
- 63 Kolinski, A.; Skolnick, J.; Yaris, R. Does reptation describe the dynamics of entangled, finite length polymer systems? A model simulation. *J. Chem. Phys.* **1987**, *86*, 1567–1585.
- 64 Svaneborg, C.; Everaers, R. Characteristic time and length scales in melts of kremer-grest bead-spring polymers with wormlike bending stiffness. *Macromolecules* **2020**, *53*, 1917–1941.
- 65 Doxastakis, M.; Theodorou, D. N.; Fytas, G.; Kremer, F.; Faller, R.; Muller-Plathe, F.; Hadjichristidis, N. Chain and local dynamics of polyisoprene as probed by experiments and computer simulations. *J. Chem. Phys.* **2003**, *119*, 6883–6894.
- 66 Farago, J.; Semenov, A. N.; Meyer, H.; Wittmer, J. P.; Johner, A.; Baschnagel, J. Mode-coupling approach to polymer diffusion in an unentangled melt. I. The effect of density fluctuations. *Phys. Rev. E* **2012**, *85*, 051806.
- 67 Farago, J.; Meyer, H.; Baschnagel, J.; Semenov, A. N. Mode-coupling approach to polymer diffusion in an unentangled melt. II. The effect of viscoelastic hydrodynamic interactions. *Phys. Rev. E* **2012**, *85*, 051807.
- 68 Farago, J.; Meyer, H.; Semenov, A. N. Anomalous diffusion of a polymer chain in an unentangled melt. *Phys. Rev. Lett.* **2011**, *107*, 178301.
- 69 Ramirez, J.; Sukumaran, S. K.; Likhtman, A. E. Significance of cross correlations in the stress relaxation of polymer melts. *J. Chem. Phys.* **2007**, *126*, 244904.
- 70 Masubuchi, Y.; Sukumaran, S. K. Cross-correlation contributions to orientational relaxations in primitive chain network simulations. *Nihon Reoroji Gakkaishi* **2013**, *41*, 1–6.
- 71 Masubuchi, Y.; Pandey, A.; Amamoto, Y. Inter-chain cross-correlation in multi-chain slip-link simulations without force balance at entanglements. *Nihon Reoroji Gakk* **2017**, *45*, 175–180.
- 72 Masubuchi, Y.; Amamoto, Y. Effect of osmotic force on orientational cross-correlation in primitive chain network simulation. *Nihon Reoroji Gakk* **2016**, *44*, 219–222.